Gain-assisted high-dimensional self-trapped laser beams at very low light levels

Hui-jun Li, Liangwei Dong, Chao Hang, and Guoxiang Huang

Phys. Rev. A **83**, 023816 — Published 23 February 2011

DOI: 10.1103/PhysRevA.83.023816

Gain-assisted high-dimensional self-trapped laser beams at very low light level

Hui-jun Li[1], Liangwei Dong[2], Chao Hang[3], Guoxiang Huang[1,3*]
[1] *Institute of Nonlinear Physics, Zhejiang Normal University, Jinhua 321004, Zhejiang, China*
[2] *Department of Physics, Zhejiang Normal University, Jinhua 321004, Zhejiang, China*
[3] *State Key Laboratory of Precision Spectroscopy, East China Normal University, Shanghai 200062, China*

(Dated: December 27, 2010)

We propose a scheme to generate high-dimensional self-trapped laser beams at a very low light intensity via atomic coherence. The system we consider is a resonant four-level atomic ensemble, working in an active Raman gain regime and at room temperature. We derive a high-dimensional nonlinear envelope equation for signal field with a specific saturable nonlinearity. We show that due to the quantum interference effect induced by a control field the imaginary part of the coefficients of the signal-field envelope equation can be much smaller than their real part. We demonstrate that the system supports gain-assisted, stable high-dimensional spatial optical solitons and long-lifetime vortices, which can be produced with light power at microwatt level.

PACS numbers: 42.65.Tg, 05.45.Yv

I. INTRODUCTION

Spatial optical solitons are special types of optical wave packets appearing as a result of interplay between diffraction and nonlinearity. The study of them is of special interest due to their rich nonlinear physics and important practical applications [1–3, 5, 32]. Up to now, most spatial optical solitons are produced in passive optical media, in which far-off resonance excitation schemes are employed in order to avoid significant optical absorption. As a result, a very high light intensity is usually needed to obtain enough nonlinearity for balancing the diffraction effect.

In recent years, much interest has focused on the wave propagation in highly resonant optical media via electromagnetically induced transparency (EIT). EIT can be used not only for suppressing optical absorption, but also for acquiring ultraslow group velocity, enhancing Kerr nonlinearity [6], and temporal [7–9] and spatial [10–13] optical solitons and vortices in resonant nonlinear systems. However, the EIT-based schemes have some inherent drawbacks, such as the probe attenuation and spreading at room temperature and the long response time due to the character of ultraslow propagation.

Parallel to the study of EIT, much attention has been also paid to the wave propagation in resonant optical media with active Raman gain (ARG) [14–23]. Contrary to EIT-based scheme which is absorptive in nature, the central idea of ARG scheme is that signal field operates in stimulated Raman emission mode, and hence attenuation of the signal field can be completely eliminated and a superluminal propagation of the signal field can be realized [14–23]. In addition, it has been shown recently by Deng and Payne [24] that a gain-assisted giant Kerr effect can also be obtained by using ARG media. Based on these results, gain-assisted temporal optical solitons of superluminal propagating velocity have been predicted [25–27]. However, up to now there is no report on the study of gain-assisted spatial optical solitons and vortices in the ARG-based systems.

In this work, we propose a scheme to generate high-D spatial optical solitons and vortices in a four-level ARG system. We derive a high-D nonlinear Schrödinger (NLS) equation for the signal-field envelope and show that, by means of the quantum interference effect induced by a control field, the imaginary part of the coefficients of the envelope equation can be much smaller than their real part. The high-D NLS equation obtained has a new type of saturable nonlinearity, which allows solutions of gain-assisted high-D spatial optical solitons and vortices. Due to the resonant character of the system, the high-D self-trapped nonlinear laser beams obtained can be produced by using very low light power.

The paper is arranged as follows. Sec. II gives a simple introduction of theoretical model and derive the high-D NLS equation. Sec. III investigates the formation and propagation of high-D spatial optical solitons and vortices, and discuss their interaction and stability. The last section summarizes main results of our work.

II. MODEL AND ENVELOPE EQUATION

The model under consideration is shown in Fig. 1. A weak signal field (with center angular frequency ω_S), a strong pump field (with center angular frequency ω_P), and a strong control field (with center angular frequency ω_C) interact resonantly with a N-type four-level system. The electric-field vector in the system is given by $\mathbf{E} = \sum_{l=P,S,C} \mathbf{e}_l \mathcal{E}_l \exp\left[i(\mathbf{k}_l \cdot \mathbf{r} - \omega_l t)\right] + \text{c.c.}$, where $\mathbf{e}_l$ ($\mathbf{k}_l$) is polarization direction (wavevector) of lth field with envelope

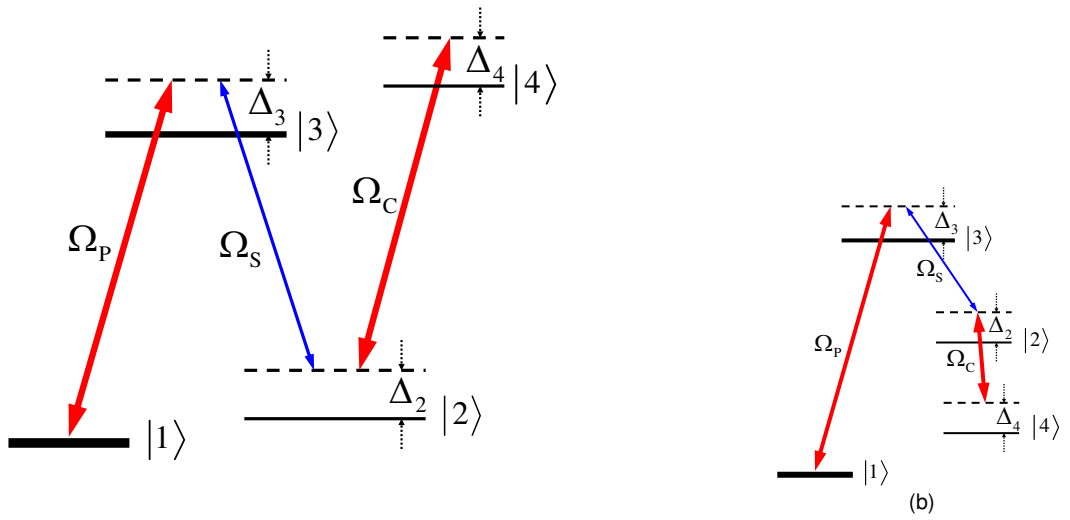

FIG. 1: (Color online) Excitation scheme of life-time broadened four-state atomic system interacting with a strong pump field (with half Rabi frequency Ω_P), a strong control field (with half Rabi frequency Ω_C), and a weak signal field (with half Rabi frequency Ω_S). $|j\rangle$ ($j = 1, 2, 3, 4$) are bare atomic states, Δ_3, Δ_2, and Δ_4 are one-photon, two-photon, and three-photon detunings, respectively.

$\mathcal{E}_l$. The Hamiltonian of the system in interaction picture reads $\hat{H}_{int} = -\hbar\sum_{j=1}^{4}\Delta_j|j\rangle\langle j| - \hbar(\Omega_P|3\rangle\langle 1| + \Omega_S|3\rangle\langle 2| + \Omega_C|4\rangle\langle 2|+\text{H.c.})$. Here $\Delta_3 = \omega_P-(\omega_3-\omega_1)$, $\Delta_2 = \omega_P-\omega_S-(\omega_2-\omega_1)$, and $\Delta_4 = \omega_P-\omega_S+\omega_C-(\omega_4-\omega_1)$ are respectively the one-, two-, and three-photon detunings; $\Omega_P \equiv (\mathbf{e}_P\cdot\mathbf{p}_{13})\mathcal{E}_P/\hbar$, $\Omega_S \equiv (\mathbf{e}_S\cdot\mathbf{p}_{23})\mathcal{E}_S/\hbar$, and $\Omega_C \equiv (\mathbf{e}_C\cdot\mathbf{p}_{24})\mathcal{E}_C/\hbar$ are respectively the half Rabi frequency of the pump, signal and control fields, with $\mathbf{p}_{ij}$ being the electric dipole matrix element associated with the transition from state $|i\rangle$ to state $|j\rangle$.

Using the Schrödinger equation $i\hbar\partial|\Psi(t)\rangle_{int}/\partial t = \hat{H}_{int}|\Psi(t)\rangle_{int}$ with $|\Psi(t)\rangle_{int} = (A_1, A_2, A_3, A_4)^T$ and under electric dipole and rotating-wave approximations, we obtain the equation of motion for A_j

$$\left(i\frac{\partial}{\partial t} + d_2\right)A_2 + \Omega_S^* A_3 + \Omega_C^* A_4 = 0, \tag{1a}$$

$$\left(i\frac{\partial}{\partial t} + d_3\right)A_3 + \Omega_P A_1 + \Omega_S A_2 = 0, \tag{1b}$$

$$\left(i\frac{\partial}{\partial t} + d_4\right)A_4 + \Omega_C A_2 = 0, \tag{1c}$$

with $\sum_{j=1}^{4}|A_j|^2 = 1$ and $d_j = \Delta_j + i\gamma_j$ ($j = 2, 3$). γ_j is the decay rate of the state $|j\rangle$.

Under slowly varying envelope approximation, the Maxwell equation for the signal field is reduced to

$$i\left(\frac{\partial}{\partial z} + \frac{1}{c}\frac{\partial}{\partial t}\right)\Omega_S + \frac{c}{2\omega_S}\nabla_\perp^2\Omega_S + \kappa A_3 A_2^* = 0, \tag{2}$$

where $\nabla_\perp^2 = \partial^2/\partial x^2 + \partial^2/\partial y^2$, $\kappa = N\omega_S|\mathbf{e}_S\cdot\mathbf{p}_{23}|^2/(2\epsilon_0\hbar c)$ with N being atomic concentration. For simplicity, the signal field has been assumed to propagate in z-direction, i.e. $\mathbf{k}_S = \mathbf{e}_z k_S$.

We assume that atoms are initially populated in the state $|1\rangle$. Since the system works at room temperature, Doppler effect resulted by thermal motion of atoms is significant. In order to suppress large gain of the signal field and the Doppler effect, we assume one-photon detuning Δ_3 is large enough. Steady-state solution of Eqs. (1) and (2) is given by $A_1^{(0)} = 1/\sqrt{1+|\Omega_P/d_3|^2}$, $A_2^{(0)} = 0$, $A_3^{(0)} = -\Omega_P/(d_3\sqrt{1+|\Omega_P/d_3|^2})$, $A_4^{(0)} = 0$. By assuming $A_j - A_j^{(0)}$ and Ω_S proportional to $\exp[i(Kz-\omega t)]$, it is easy to get the linear dispersion relation of the signal field

$$K(\omega) = \frac{\omega}{c} - \frac{\kappa|A_3^{(0)}|^2(\omega - d_4^*)}{|\Omega_C|^2 - (\omega - d_2^*)(\omega - d_4^*)}, \tag{3}$$

where ω and K are deviation of frequency and wavevector of the signal field, respectively. Fig. 2 shows the real part

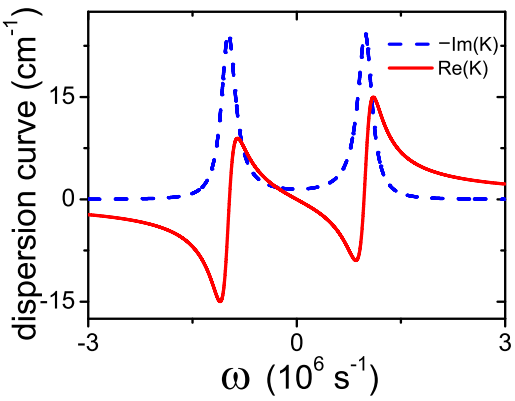

FIG. 2: (Color online) Real part Re$K(\omega)$ (solid line) and negative imaginary part $-\mathrm{Im}K(\omega)$ (dashed line) of the linear dispersion relation of the signal field as functions of ω.

Re$K(\omega)$ (solid line) and the negative imaginary part $-\mathrm{Im}K(\omega)$ (dashed line) of K as a function of ω with realistic system parameters for ^{87}Rb atoms [24]. We see that $-\mathrm{Im}K(\omega)$ displays a structure of gain spectrum hole, where signal-field gain is largely suppressed. The width of the gain spectrum hole is proportional to the intensity of the control field. The physical reason for the appearance of such gain spectrum hole is the quantum interference effect induced by the control field [27, 28].

We focus on steady-state regime of the system, in which time-derivative terms in Eqs. (1) and (2) can be neglected. Such regime can be realized under the condition $|d_j|\tau_0 \gg 1$, where τ_0 is the pulse length of the signal field. In this case, using Eq. (1) we obtain $A_1 = DA_3/(\Omega_P D_1)$, $A_2 = d_4\Omega_S^* A_3/D_1$, $A_4 = -\Omega_C\Omega_S^* A_3/D_1$, with $|A_3|^2 = \left(1 + |d_4\Omega_S/D_1|^2 + |D/(\Omega_P D_1)|^2 + |\Omega_C\Omega_S/D_1|^2\right)^{-1}$, $D_1 = |\Omega_C|^2 - d_2 d_4$, and $D = -d_3 D_1 - d_4|\Omega_S|^2$. Then Eq. (2) reduces to the (2+1)-D NLS equation with saturable nonlinearity

$$i\frac{\partial\Omega_S}{\partial z} + \frac{c}{2\omega_S}\nabla_\perp^2\Omega_S + \frac{\kappa d_4^* D_1}{G}\frac{\Omega_S}{1+\alpha|\Omega_S|^2+\beta|\Omega_S|^4} = 0, \tag{4}$$

with $\alpha = \left[|d_4|^2 + |\Omega_C|^2 + 2|d_4/\Omega_P|^2\mathrm{Re}(d_3 D_1/d_4)\right]/G$, $\beta = |d_4/\Omega_P|^2/G$, and $G = |D_1|^2(1+|d_3/\Omega_P|^2)$.

In linear approximation, the signal beam spreads during propagation due to the diffraction of the system. In order to arrest such spreading and obtain a stable signal-beam propagation, a natural way is to use the saturable nonlinear effect of the system. To explore such possibility we write Eq. (4) into the dimensionless form

$$i\frac{\partial u}{\partial s} + \left(\frac{\partial^2}{\partial\xi^2} + \frac{\partial^2}{\partial\eta^2}\right)u + \mathrm{Re}(\delta)\frac{u}{1+\sigma|u|^2+\zeta|u|^4} = P[u], \tag{5}$$

where $s = z/L_D$, $(\xi,\eta) = (x,y)/R_\perp$, and $u = \Omega_S/U_0$, with $L_D(\equiv 2R_\perp^2\omega_S/c)$, $R_\perp$, and U_0 being respectively characteristic diffraction length, beam radius, and half Rabi frequency of the signal field. The function on the right hand side (RHS) of Eq. (5) is defined by $P[u] = -i\mathrm{Im}(\delta)u/[1+\sigma|u|^2+\zeta|u|^4]$. The coefficients in Eq. (5) are given by $\sigma = U_0^2\alpha$, $\zeta = \beta U_0^4$, and $\delta = \mathrm{Re}(\delta) + i\mathrm{Im}(\delta)$, with $\mathrm{Re}(\delta) = \Delta_4\kappa D_1 L_D/G$ and $\mathrm{Im}(\delta) = -\gamma_4\kappa\gamma_4 D_1 L_D/G$. Notice that σ and ζ are real, but δ is complex. Notice that since $\mathrm{Im}\delta < 0$, the term $P[u]$ in Eq. (5) is not an absorption but a *gain* one.

Now we make an estimation of realistic values of the coefficients appeared in Eq. (5). We consider a typical warm atomic vapor of ^{87}Rb used in Ref. [24]. System parameters are given by $\gamma_2 = 150\,\mathrm{Hz}$, $\gamma_3 = 250\,\mathrm{MHz}$, $\gamma_4 = 250\,\mathrm{kHz}$, $\kappa = 7.04\times10^9\,\mathrm{cm^{-1}s^{-1}}$, and $\omega_S = 2.37\times10^{15}\,\mathrm{s^{-1}}$. Other parameters are chosen as $\Delta_2 = 0$, $\Delta_3 = -2.0\times10^9\ \mathrm{s^{-1}}$, $\Delta_4 = -3.0\times10^8\ \mathrm{s^{-1}}$, $\Omega_P = 8.0\times10^7\ \mathrm{s^{-1}}$, $\Omega_C = 6.0\times10^7\ \mathrm{s^{-1}}$, and $R_\perp = 4.0\times10^{-3}\,\mathrm{cm}$. With these parameters, we obtain $L_D = 2.53$ cm, $U_0 = 1.04\times10^8\ \mathrm{s^{-1}}$, $\sigma = 1.0$, and $\zeta = 0.19$, and $\delta = -11.66 - 0.01i$. Because $\mathrm{Im}(\delta) \ll \mathrm{Re}(\delta)$, the term $P[u]$ on the RHS of Eq. (5) can be taken as a perturbation. Consequently, in leading order approximation Eq. (5) becomes a NLS equation without gain. Such result is interesting because in usual undriven resonant systems one obtains envelope equations with very strong gain or dissipation, i.e. the coefficients of the envelope equations have imaginary parts that are of the same order of corresponding real parts. The physical reason of so small imaginary part in the coefficients of the envelope equation (5) is due to the quantum interference effect induced by the control field.

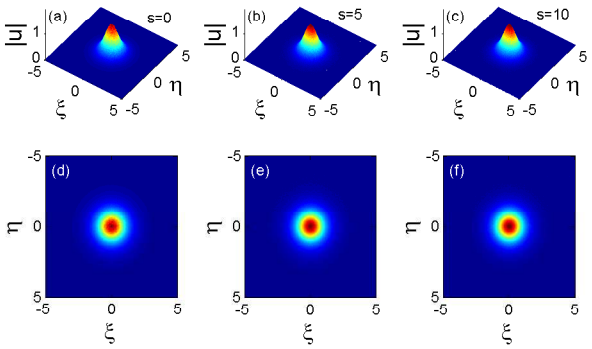

FIG. 3: (Color online) Soliton profile $|u|$ as a function of coordinates ξ, η, and s, obtained by numerically solving Eq. (5). (a): Initial profile of the soliton ($s = 0$). (b) and (c): Soliton profiles when propagating to five ($s = 5$) and ten ($s = 10$) diffraction lengths, respectively. (d), (e), and (f): 2D projection plots correspond to panels (a), (b), and (c), respectively.

NLS equations with saturable nonlinearity have been studied for many years [29, 30, 33]. In many cases investigated so far, the term related to saturable nonlinearity is of the form $f(I)u$, with $I = |u|^2$. Usually, in non-resonant systems $f(I)$ takes the form $n_0/(1+I/I_0)$, or $n_2 I/(1+I/I_0)$, with n_0, n_2, and I_0 being constants [2, 3, 5, 32]. In resonant EIT systems, $f(I)$ takes the form $n_0/(1 + I/I_0)$ (three-level) [12], or a very complicated form (four-level) [10]. However, the saturable nonlinearity we obtained in the present four-level ARG system is very specific, which has the form $f(I) = n_0/(1 + I/I_0 + I^2/I_1^2)$, with n_0, I_0 and I_1 being constants.

III. HIGH-D SPATIAL OPTICAL SOLITONS AND VORTICES

We now investigate the possibility of spatial optical solitons and vortices supported by saturable nonlinearity, based on the NLS equation (5). Our strategy is as follows. We first get soliton or vortex solutions in the leading-order approximation (i.e. the perturbation $P[u]$ is set to zero). Then, we solve Eq. (5) by taking the leading-order solutions as initial conditions to obtain the soliton or vortex solutions of Eq. (5) numerically. In fact, the solutions in the leading-order approximation are already quite accurate because $\mathrm{Im}(\delta)/\mathrm{Re}(\delta) \approx 10^{-3}$.

In the leading-order approximation, the solution of Eq. (5) has the from $u = \Psi(r)\exp[i(\mu + \mathrm{Re}(\delta))s + im\phi]$, here $r^2 = \xi^2 + \eta^2$, μ is propagation constant, and $m(\geq 0)$ is winding number. The solution for $m = 0$ corresponds to a soliton, while for $m \neq 0$ the solution corresponds to a vortex with topological charge m. Boundary conditions are $\partial\Psi/\partial r = 0$ at $r = 0$ and $\Psi = 0$ at $r \to \infty$ for $m = 0$ (for solitons), or $\Psi = 0$ at $r = 0$ and $r \to \infty$ for $m > 0$ (for vortices).

A. Solitons

The soliton solution corresponds to the winding number $m = 0$. We solve Eq. (5) by using Newton iteration method [34], with $\mu = 2.0$, $\delta = -11.6 - 0.01i$, $\sigma = 1.0$, and $\zeta = 0.19$. Fig. 3 shows the result of our numerical simulation. Panels (a), (b), and (c) of the figure are soliton profiles for $s = 0$, $s = 5$, and $s = 10$ (in unit of $L_D = 2.53$ cm), respectively. Panels (d), (e), and (f) are 2D projection plots corresponding to panels (a), (b), and (c), respectively. For checking the stability of the soliton, in the simulation we have added a small randomness ρ_{ran} to the initial condition, i.e. $u = u_{\mathrm{sol}}(1 + \rho_{\mathrm{ran}})$, with $|\rho_{\mathrm{ran}}| = 0.1$. From Fig. 3 we see the soliton keeps its shape after propagating to ten diffraction length (i.e. $s = 10$). Hence Eq. (5) admits indeed soliton solution and this solution is fairly stable during propagation.

We have also investigated collisions between two solitons by using an accelerated imaginary-time evolution method [35]. Shown in Fig. 4 are profiles of amplitude $|u|$ as function of ξ, η, and s for two-soliton collisions. The physical parameters are chosen as the same as Fig. 3. The lower part of the figure is corresponding projecting (to ξ-η plane) plots of the upper part. Note that in the upper part of the figure, 3D plots have been projected into the $\eta = 0$ plane. From the figure we see that soliton collisions display elastic character; two solitons are attractive for $\Delta\phi = 0$, but repulsive for $\Delta\phi = \pi$.

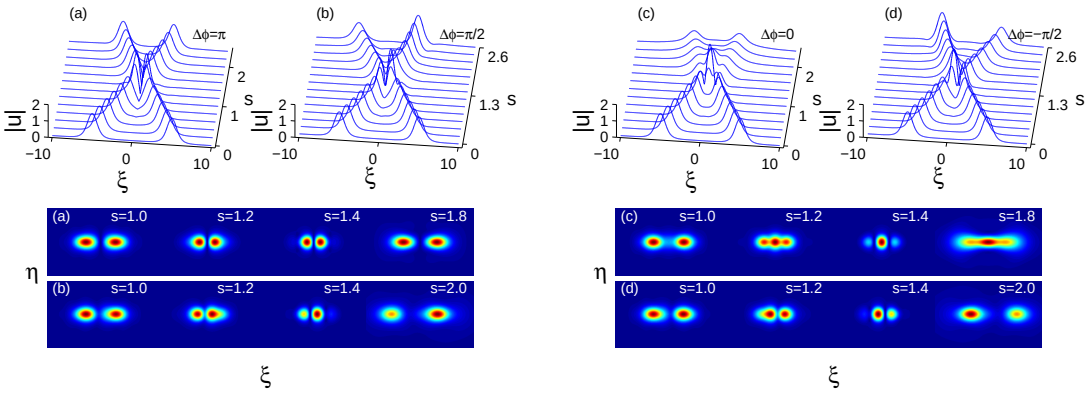

FIG. 4: (Color online) Profiles of amplitude $|u|$ for two-soliton collisions as function of ξ and s (projection to $\eta = 0$ plane has been taken). Panels (a), (b), (c) and (d) are for collisions of two solitons with initial relative phase $\Delta\phi = \pi$, $\pi/2$, 0 and $-\pi/2$, respectively. The lower part of the figure is corresponding projection (to ξ-η plane) plots of the upper part.

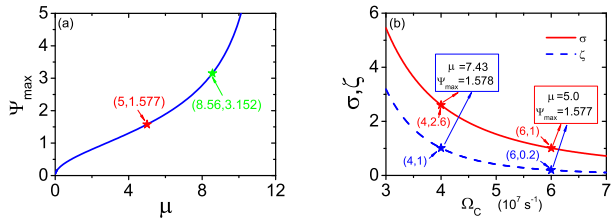

FIG. 5: (Color online) (a): $\Psi_{\max}$ as a function of propagation constant μ, with $\Omega_C = 6.0\times10^7$ s^{-1}. The vortex corresponding to the point $(\mu, \Psi_{\max})$=(8.56,3.152) in the curve has a longer lifetime than the vortex corresponding to the point $(\mu, \Psi_{\max})$=(5,1.577). (b): Curves of saturation parameters σ (solid line) and ζ (dashed line) as functions of Ω_C. The point (4.0,2.6) in the σ-curve and the point (4,1) in the ζ-curve correspond to $(\mu, \Psi_{\max}) = (7.43, 1.578)$. The point (6.0,1.0) in the σ-curve and the point (6.0,0.2) in the ζ-curve correspond to $(\mu, \Psi_{\max}) = (5.0, 1.577)$. The vortex corresponding to $(\mu, \Psi_{\max}) = (7.43, 1.578)$ has a longer lifetime than the vortex corresponding to $(\mu, \Psi_{\max}) = (5.0, 1.577)$.

It is easy to get the peak generation power of the spatial optical soliton obtained above, which is given by $\bar{P}_{\max} = 2\epsilon_0 c n_S S_0(\hbar/|\ \mathbf{p}_{23}|)^2 U_0^2 |u_{\max}|^2$, with n_S and S_0 being the reflective index and the cross-section area of the signal beam, respectively. Taking $S_0 = \pi R_\perp^2 \approx 0.5\times10^{-4}$ cm^2, $|\ \mathbf{p}_{23}| = 2.1\times10^{-27}$ cm C, and using the other parameters given above, we obtain $\bar{P}_{\max} = 2.32\,\mu$W. Hence, the spatial optical soliton in the present system can be generated at very low light power, which is much different from the optical soliton generation schemes using passive media, where much higher generation power is required.

B. Vortices

It is well known that vortices of high-D NLS equations are generally unstable. However, saturable nonlinearity may be used to effectively suppress such instability [29–33]. For a non-resonant passive system, saturation intensity is very large, and saturation parameters of the system are fixed. However, our present system is a resonant active one, the situation is thus quite different. On the one hand, due to the resonant character of the system, the saturation intensity is very small. This can be seen as follows. From Eq. (5), the saturable nonlinearity can be obtained by setting $\sigma|u_{\rm sat}|^2 \approx 1$, which gives the saturable electric field of the signal beam as $|E_{\rm sat}| = \hbar U_0/|\mathbf{p}_{23}|$. Using the numerical values of the physical parameter given above, we obtain $|E_{\rm sat}| \approx 5$ V/m. On the other hand, the active character of the present system provides us many adjustable parameters, which can be manipulated to reduce the saturation intensity and increase vortex lifetime. In the following, we shall discuss only how to increase the vortex lifetime by adjusting the half control-field Rabi frequency Ω_C. From Eq. (5) we know that the coefficients δ, σ, and ζ depend on Ω_C, and hence the solution parameters of vortices, i.e. the propagation constant μ and $\Psi_{\max}$(the maximum value of Ψ), depend also on Ω_C.

Shown in Fig. 5(a) is the relation between $\Psi_{\max}$ and μ, with $\Omega_C = 6.0\times10^7$ s^{-1}. The vortex correspond-

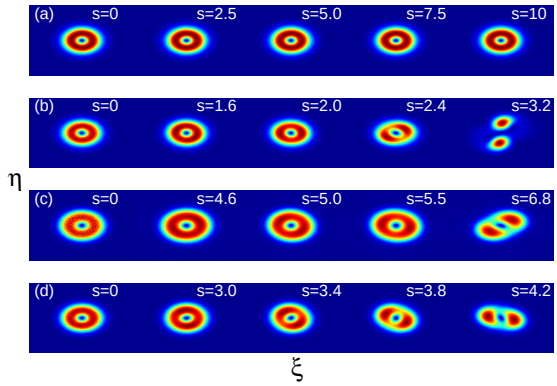

FIG. 6: (Color online) Evolution of amplitude $|u|$ of $m = 1$ vortex as a function of (ξ, η), with different propagating distance s. (a): Evolution corresponding to the point $(\mu, \Psi_{\max})$=(5,1.577) of Fig. 5(a) without adding any random perturbation. (b): Evolution when a random perturbation is added into the initial condition. The vortex keeps its shape till propagating to $s = 2.4$, but it deforms after $s = 2.4$ and then disintegrates into two solitons. (c): Evolution of large-amplitude vortex corresponding to the point $(\mu, \Psi_{\max})$=(8.56,3.152) of Fig. 5(a). The vortex has a longer lifetime comparing with the case shown in panel (b), but it splits into two solitons at large s. (d): Evolution corresponding to $\Omega_C = 4.0 \times 10^7$ s, which corresponds to $(\mu, \Psi_{\max}) = (7.43, 1.578)$ of Fig. 5(b).

ing to the point $(\mu, \Psi_{\max})$=(8.56,3.152) in the curve is more stable than the vortex corresponding to the point $(\mu, \Psi_{\max})$=(5,1.577). Shown in Fig. 5(b) are curves of saturation parameters σ (solid line) and ζ (dashed line) as functions of Ω_C for fixed parameters $\Delta_2 = 0$, $\Delta_3 = -2.0 \times 10^9$ s^{-1}, $\Delta_4 = -3.0 \times 10^8$ s^{-1}, and $\Omega_P = 8.0 \times 10^7$ s^{-1}. Since the saturation intensity of the signal field is inversely proportional to σ and ζ, from the figure we see that one can reduce the saturation intensity by decreasing Ω_C. In the figure, by choosing 10^7 s^{-1} as the unit of Ω_C we have illustrated the point (Ω_C, σ)=(4.0,2.6) in the σ-curve and the point (Ω_C, ζ)=(4.0,1.0) in the ζ-curve. Using the values of Ω_C, σ and ζ at these points, we obtain $(\mu, \Psi_{\max}) = (7.43, 1.578)$, which has been indicated in the insetted up-left square in the figure; we have also illustrated the point (Ω_C, σ)=(6.0,1.0) in the σ-curve and the point (Ω_C, ζ)=(6.0,0.2) in the ζ-curve, which correspond to $(\mu, \Psi_{\max}) = (5.0, 1.577)$ that is indicated in the insetted bottom-right square. The vortex corresponding to $(\mu, \Psi_{\max}) = (7.43, 1.578)$ has a longer lifetime comparing with the vortex corresponding to $(\mu, \Psi_{\max}) = (5.0, 1.577)$. All these predications have been verified by numerical simulations.

In Fig. 6 we have shown the evolution of $|u|$ for $m = 1$ vortex with different distance s. Panel (a) of the figure corresponds to the point $(\mu, \Psi_{\max})$=(5,1.577) of Fig. 5(a) without adding any random perturbation to initial condition. No deformation of the vortex is found after propagating to $s = 10$. However, when a random perturbation $\rho_{\rm ran}$ (with $|\rho_{\rm ran}| = 0.158$) is added into the initial condition, i.e. $u = u_{vor}(1 + \rho_{\rm ran})$, the vortex is stable till propagating to $s = 2.4$, but it deforms after $s = 2.4$ and disintegrates into two solitons, as shown clearly in panel (b). Plotted in panel (c) of the figure is the result of the evolution of large-amplitude $m = 1$ vortex corresponding to the point (8.56,3.152) of Fig. 5(a). In this case, vortex has a longer lifetime in comparison with the case shown in panel (b) because the vortex can propagates to a longer distance even a random perturbation is added into the initial condition. Of course, it splits into two solitons at large distance.

All evolution figures in panels (a), (b), and (c) are obtained for $\Omega_C = 6.0 \times 10^7$ s. In order to demonstrate the effect of different saturation parameters, in the panel (d) of Fig. 6 we have shown the evolution of $m = 1$ vortex for $\Omega_C = 4.0 \times 10^7$ s, which corresponds to $(\mu, \Psi_{\max}) = (7.43, 1.578)$ of Fig. 5(b). We see that in this case the vortex is also relatively stable comparing with that shown in the panel (b).

Shown in Fig. 7 are the evolution plots of the $m = 2$ vortex for four different propagating distance s. Panel (a) in the figure is the vortex evolution for $(\mu, \Psi_{\max}) = (5, 1.565)$ without adding any random perturbation to the initial condition. We see that, different from the $m = 1$ vortex, the $m = 2$ vortex can not keep its shape even with no random perturbation added into the initial condition. At $s = 6.25$, the vortex splits into four solitons. When a random perturbation $\rho_{\rm ran}$ (with $|\rho_{\rm ran}| = 0.157$) is added into the initial condition, the vortex displays instability in earlier stage ($s = 2.4$). At $s = 2.8$, it splits into four solitons as shown in panel (b) of the figure. Panel (c) shows the result of the evolution of large-amplitude $m = 2$ vortex corresponding to $(\mu, \Psi_{\max}) = (8.56, 3.152)$. We see that the large-amplitude vortex is relatively stable comparing with that of the (small-amplitude) vortex of panel (b). However, it disintegrates into three (not four) solitons at long evolution distance.

We have also simulated the evolution of the $m = 2$ vortex by changing the Rabi frequency of the control field. Shown in panel (d) is the evolution of the $m = 2$ vortex for $\Omega_C = 4.0 \times 10^7$ s, which corresponds to $(\mu, \Psi_{\max}) = (7.43, 1.566)$.

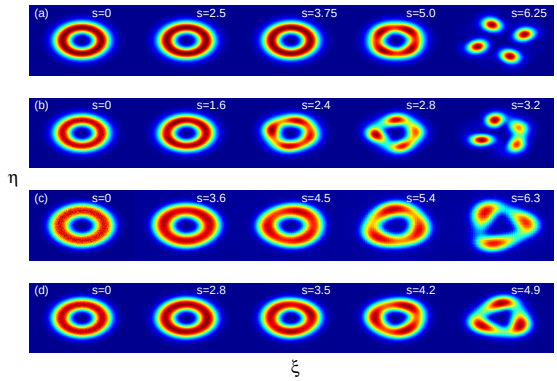

FIG. 7: (Color online) Evolution plots of the $m = 2$ vortex as functions of (ξ, η), with different propagating distance s. (a): Vortex evolution based on Eq. (5) for $(\mu, \Psi_{\max}) = (5, 1.565)$ without adding any random perturbation to initial condition. (b): Vortex evolution when a random perturbation is added into the initial condition. (c): Evolution of large-amplitude $m = 2$ vortex corresponding to $(\mu, \Psi_{\max}) = (8.56, 3.152)$. (d): Evolution of $m = 2$ vortex corresponding to $\Omega_C = 4.0 \times 10^7$ s, which corresponds to $(\mu, \Psi_{\max}) = (7.43, 1.566)$.

We see that the vortex in this case is also relatively stable in comparison with that shown in the panel (b). Generally, by manipulating the parameters of the system, we can control the lifetime of the vortex freely. In particular, when the control-field intensity decreases a small amount, the lifetime of the vortex can increase significantly. In addition, it is easy to show that the peak generation powers of the $m = 1$ and $m = 2$ vortices are also at microwatt level.

IV. DISCUSSION AND SUMMARY

Generally, the vortices found in the system are unstable, mainly due to symmetry-breaking azimuthal perturbations. However, as shown above the instability can be very weak, i.e. the vortices can have long lifetime and hence observable in experiment and useful for practical applications. Because our system is an active one, one can control the weak instability of the vortices by manipulating the system parameters at will. In addition, there exists a parameter domain in which the vortices are stable, which can be illustrated as follows. Notice that Eq. (5), after making the transformation $u = v \exp(i\delta s)$, can be reduced into the following cubic-quintic NLS equation

$$i\frac{\partial v}{\partial s} + \left(\frac{\partial^2}{\partial \xi^2} + \frac{\partial^2}{\partial \eta^2}\right) v - \delta\sigma|v|^2 v - \delta(\zeta - \sigma^2)|v|^4 v = 0 \tag{6}$$

if $\sigma|u|^2 + \zeta|u|^4 \ll 1$, which can be realized when (i)the signal field is weak and (ii)the saturation intensity is large, which can be achieved easily by selecting the system parameters. Under the condition

$$\delta\sigma = -1, \quad \delta(\zeta - \sigma^2) = 1, \tag{7}$$

Eq. (6) can be transferred into the standard cubic-quintic NLS equation $i\frac{\partial v}{\partial s} + \left(\frac{\partial^2}{\partial \xi^2} + \frac{\partial^2}{\partial \eta^2}\right) v + |v|^2 v - |v|^4 v = 0$, which admits stable vortices [31]. The condition (7) can be easily fulfilled in our system. For instance, by choosing $\Delta_3 = -1.0 \times 10^9$ s^{-1}, $\Delta_4 = -1.69\Delta_3$, $\Omega_P = \Omega_C = -0.1\Delta_3$, $U_0 = -0.44\Delta_3$, $R_\perp = 2.516 \times 10^{-3}$ cm, one obtains $\sigma \approx -0.09$, $\zeta \approx 0.10$, and thus the condition (7) is well satisfied. In this parameter domain, the vortices are very stable, which has been verified in our numerical simulation.

In conclusion, we have proposed a scheme for generating high-D self-trapped laser beams at a very low light intensity via atomic coherence. The system we have considered is an ensemble of resonant four-level atoms, working in an active Raman gain regime and at room temperature. We have derived a (2+1)-D NLS equation for the signal-field envelope with a specific saturable nonlinearity. We have shown that, due to the quantum interference effect induced by a control laser field, the imaginary part in coefficients of the NLS equation can be much smaller than their real part. We have demonstrated that the system supports stable high-D spatial optical solitons and long-lifetime vortices, which can be produced with light power at microwatt level. The results presented here may be useful for understanding the nonlinear property of coherent atomic systems and guiding experimental findings of spatial solitons and vortices with very low generation power, which may have potential applications in optical information processing and engineering.

Acknowledgments

Authors thank Vladimir V. Konotop for useful discussions and Jianke Yang for helpful suggestions on our numerical simulations. This work was supported by the NSF-China under Grant Nos. 10874043, 10947137 and 10974181, and by the NSF-Zhejiang province of China under Grant Nos. Y6100355.

[1] G. I. Stegeman and M. Segev, Science **286**, 1518 (1999).
[2] Y. S. Kivshar and G. P. Agrawal, *Optical Solitons: From Fibers to Photonic Crystals* (Academic Press, New York, 2003).
[3] Y.-F. Chen, K. Beckwitt, and F. W. Wise, Phys. Rev. E **70**, 046610 (2004).
[4] B. A. Malomed, D. Mihalache, F. Wise, and L. Torner, J. Phys. B: Quantum Semiclass. Opt. **7**, R53 (2005).
[5] M. J. Paz-Alonso and H. Michinel, Phys. Rev. Lett. **94**, 093901 (2005).
[6] M. Fleischhauer, A. Imamoglu, and J. P. Marangos, Rev. Mod. Phys. **77** 633 (2005).
[7] Y. Wu and L. Deng, Phys. Rev. Lett. **93**, 143904 (2004).
[8] G. Huang, L. Deng and M. G. Payne, Phys. Rev. E. **72**, 016617 (2005).
[9] C. Hang and G. Huang, Phys. Rev. A **77**, 033830 (2008).
[10] T. Hong, Phys. Rev. Lett. **90**, 183901 (2003).
[11] H. Michinel and M. J. Paz-Alonso, Phys. Rev. Lett. **96**, 023903 (2006).
[12] C. Hang, G. Huang, and L. Deng, Phys. Rev. E **73**, 046601 (2006).
[13] A. Alexandrescu, H. Michinel, and V. M. Perez-Garcia, Phys. Rev. A **79**, 013833 (2009).
[14] R. Y. Chiao and A. M. Steinberg, in *Progress in Optics*, edited by E. Wolf (Elsevier, Amsterdam, 1997), p. 345.
[15] L. J. Wang, A. Kuzmich, and A. Dogariu, Nature (London) **406**, 277 (2000).
[16] M. S. Bigelow, N. N. Lepeshkin, and R. W. Boyd, Science **301**, 200 (2003).
[17] M. D. Stenner, D. J. Gauthier, and M. A. Neifield, Nature **425**, 695 (2003).
[18] R. G. Ghulghazaryan and Y. P. Malakyan, Phys. Rev. A **67**, 063806 (2003).
[19] K. Kim, H. S. Moon, C. Lee, S. K. Kim, and J. B. Kim, Phys. Rev. A **68**, 013810 (2003).
[20] L.-G. Wang, N.-H. Liu, Q. Ling, and S.-Y. Zhu, Phys. Rev. E **68**, 066606 (2003).
[21] M. Janowicz and J. Mosttowski, Phys. Rev. E **73**, 046613 (2006).
[22] K. Jiang, L. Deng, and M. G. Payne, Phys. Rev. A **74**, 041803(R) (2006).
[23] J. Zhang, G. Hernandez, and Y. Zhu, Opt. Lett. **31**, 2598 (2006).
[24] L. Deng and M. G. Payne, Phys. Rev. Lett. **98**, 253902 (2007).
[25] G. Huang, C. Hang, and L. Deng, Phys. Rev. A. **77**, 011803(R) (2008).
[26] H.-j. Li, C. Hang, G. Huang, and L. Deng, Phys. Rev. A **78**, 023822 (2008).
[27] C. Hang and G. Huang, Opt. Express **18**, 2952 (2010).
[28] G. S. Agarwal and S. Dasgupta, Phys. Rev. A **70**, 023802 (2004).
[29] W. J. Firth and D. V. Skryabin, Phys. Rev. Lett. **79**, 2450 (1997).
[30] D. V. Skryabin and W. J. Firth, Phys. Rev. E **58**, 3916 (1998).
[31] I. Towers, A. V. Buryak, R. A. Sammut, B. A. Malomed, L.-C. Crasovan, D. Mihalache, Phys. Lett. A **288**, 292 (2001).
[32] B. A. Malomed, D. Mihalache, F. Wise, and L. Torner, J. Opt. B **7**, R53 (2005), and references therein.
[33] A. S. Desyatnikov, Y. S. Kivshar, and L. Torner, in *Progress in Optics*, edited by E. Wolf (Elsevier Science, Amsterdam, 2005), Vol. **47**, Chap. 6, p. 1, and references therein.
[34] J. Yang, J. Comp. Phys. **228**, 7007 (2009).
[35] J. Yang and T. I. Lakoba, Stud. Appl. Math. **120**, 265(2008).